Intelligent Service Robotics
https://doi.org/10.1007/s11370-022-00420-y

ORIGINAL RESEARCH PAPER

Enabling landings on irregular surfaces for unmanned aerial vehicles via a novel robotic landing gear

TsungHsuan Huang[1] · **Armagan Elibol**[1] · **Nak Young Chong**[1]

Received: 29 July 2021 / Accepted: 13 March 2022

Abstract
Unmanned aerial vehicles (UAVs) have been attracting much attention and changing our daily lives. Recent technological advances in the development of UAVs have drastically increased both their general capabilities and areas of application. Among many others, one of the areas that benefits immediately from using UAVs could be remote inspection, since they can provide an alternative means of access to structures and collect data from locations difficult to reach for human inspectors. Lately, wall-climbing UAVs outfitted with contact-type sensors have been proposed to collect data for the periodic inspection and maintenance of buildings. However, the major drawback is that they can be used only for flat surfaces. In this paper, we present a lightweight robotic landing gear for enabling UAVs to land on irregular surfaces, without affecting the on-board flight control system that keeps the UAV in level flight during the entire mission. Our novel design uses a vacuum system for robotic landing gear to attach to the surface, and the movable counterweight composed of a vacuum motor and other control components to balance the flight. To lighten the total weight of UAV, the proposed robotic landing gear system has only one servo motor for gear operation and a passive mechanical structure that guides the vacuum suction cup at the frontal robotic legs to adapt to different shapes of surfaces. We present details of a prototype mechanism and landing experimental results under different scenarios generated within our laboratory environment.

Keywords Unmanned aerial vehicles · Nondestructive inspection · Landing gear · Vacuum suction · Passive controlled structural mechanism

Mathematics Subject Classification 70B15 · 70E60

1 Introduction

Nowadays robotic vehicles are increasingly used in a variety of applications and changing our daily life. With the improvements in their capabilities (e.g., mobility, exploration, data collection, autonomy, and many others), they have been viable for the tasks that need to take place in hazardous environments. Periodic maintenance and inspection of man-made high-rise structures is one of such tasks. It is widely known that wall-climbing robots (WCRs) were proposed to use for inspection and cleaning of buildings, replacing long reach fixed based manipulators. However, the moving speed of WCRs is usually relatively slow, which often needs to be provided by roof cables and winches. This significantly limits the scope of applications of WCRs. Notably, the unmanned aerial vehicle (UAV) technology has made astonishing progress in recent years, and its application areas are not only limited to aerial photography, entertainment, and similar others. An increasing number of tasks requiring UAVs to physically interact with their surroundings have been demonstrated (e.g., inspection [8, 17] and agriculture [5, 6, 12]). In light of recent technological advances of UAVs in payload capacity, endurance, flight stability and control, and user interface, as well as the decline in the price of hardware platform, UAVs begin to be used for civil operations under the related regulations and guidance. Therefore, UAVs are deemed as an appropriate alternative for the maintenance and inspection

✉ TsungHsuan Huang
huang910008@gmail.com

Armagan Elibol
aelibol@jaist.ac.jp

Nak Young Chong
nakyoung@jaist.ac.jp

[1] School of Information Science, Japan Advanced Institute of Science and Technology, Nomi, Ishikawa 923-1292, Japan

Table 1 A comparison of existing surface attaching systems for UAVs

Design	Feature	Advantage	Disadvantage
[21]	Micro spines (Landing)	UAV stops when landed	No landing on irregular surfaces
		Efficient battery usage	Limited payload due to micro spines
[11] [18] [27]	Wheels (Attaching)	Mobility on the surface	Difficult to be kept at a fixed position
		Agile than wall-climbing	
[7] [9] [10]	Manipulators (Attaching)	Accurate attaching position	Mobility difficulty on irregular surfaces
		Using contact-type sensors	Balance issues due to the arm length
[14] [19]	UAV itself (Attaching)	No extra mechanism needed	Difficult to attach to irregular surfaces
			And install with contact-type sensors

tasks to overcome the aforementioned issues with WCRs. For this reason, we propose a lightweight robotic landing gear prototype that enables the UAV to attach ideally to any shape of the surface.

Different application-oriented platforms [13, 22] have been developed in response to the nature and needs of bridge inspection tasks. As mentioned above, off-the-shelf or custom-built UAV platforms can be potentially utilized for nondestructive inspection and maintenance of man-made high-rise structures, bridges, and bodies of airplanes. There have already been several attempts in remote inspection (e.g., wall, dam, and many others [23, 25]), in which UAVs were an indispensable tool thanks to their ability to obtain data through optical sensors available on board. Specifically, for nondestructive inspection on high-rise buildings, there is always the risk of being affected by the wind. Therefore, it is of utmost importance to keep the UAV attached to the target surface securely and obtain the necessary data correctly.

This paper proposes a novel robotic landing gear for off-the-shelf UAVs, which aims to enable it to land on any shape of surfaces. This design uses only one servo motor to reduce weight and power consumption, combined with a universal joint and multi-link design to achieve a high level of efficiency in irregular surface landing. This robotic landing gear with a mechanical structure weighs less than 1 kilogram. Using only one servo motor and two vacuum motors can allow a UAV to land on different shapes of surfaces. In general, if mobile robots should be endowed with the capability of performing a large set of movements, it means that multiple motors are incorporated into the drive mechanism, which will cause an increases in total power consumption and weight. In order to keep the weight a minimum, we have adopted passive mechanical structures, minimizing the number of motors while keeping the expected function unaffected. This makes it possible for a UAV outfitted with the proposed landing gear to access complex and dangerous environments, such as industrial facilities, disaster sites after earthquakes, and similar others, and collect data in an energy-efficient manner.

The rest of the paper is organized as follows. Section 2 briefly overviews the existing designs that enable UAVs to perform some tasks on surfaces. Section 3 presents our proposed landing gear in detail. In Sect. 4, we present our findings derived from a series of experiments on different surface landing. The last section is devoted to draw conclusions and suggest future research directions.

2 Related work

Remote inspection and maintenance is one of the important areas in which robotic platforms can be used intensively. For example, mobile robots can provide a viable solution in the infrastructure inspection sector, since they can move or even fly over vertical and sloped surfaces to reach high-risk locations in civil structures [3]. Specifically, WCRs are a specialized kind of mobile robots potentially used in periodic inspections and maintenance [4]. WCRs may have higher payload carrying capability and better endurance. However, they are usually unwieldy and apply a lower speed limit. Therefore, in recent years, many wall-climbing UAVs have gradually replaced WCRs in bridge inspections and other high-altitude tasks [1, 24].

A variant of WCR based on the UAV platform is called as PRWCR (propeller-type wall-climbing robot) [16]. Several different methods for attaching to the target surface have been proposed such as micro-spine [21], manipulator [9], vacuum system [26], and the power of UAV itself [19]. The feature, advantages, and disadvantages of various designs are briefly summarized in Table 1. PRWCRs are used instead of conventional UAVs, since many tasks such as cleaning or inspection require secure contact with the target surface. However, the existing PRWCRs are often designed and developed for applications on vertical walls and usually cannot be used on discontinuous or irregular surfaces effectively, which still limits the usages of UAVs on such robots. In order to endow off-the-shelf UAVs with the capability of landing on

arbitrarily shaped surfaces, a viable solution is the development of a landing gear mounted underneath a UAV that can adapt to complex landing surface conditions. It is highly desirable due to the limited battery capacity that the landing gear configuration be controlled by a small number of motors, without affecting the flight control system or requiring a sophisticated flight control during the entire mission.

In [17], Myeong *et al*. added an additional structure to the UAV. To effectively use the thrust force of the UAV, they control the structure to adjust the angle between the UAV and the wall. However, the purpose of this work is to make the UAV attach to the wall instead of landing. Therefore, this design can neither turn off the power of the UAV nor fixed at the same position for a long time. In [21], a UAV capable of perching and climbing with passive technology was proposed through the cooperative robotic platform with a 2 degrees-of-freedom climbing mechanism. Although their platform was lightweight and could perch on rough exterior surfaces, it was not able to adapt to uneven surfaces. Furthermore, the payload was also comparatively low for installing additional sensors and/or other equipment for different tasks. In contrast, our design attempts to use a set of vacuum suction cups as an alternative to the aforementioned climbing mechanism. This makes the platform secure a better payload capability, more stable on the surface, and more powerful to perch on the surface. For irregular surfaces landing, Paul *et al*. proposed a UAV equipped with 3 manipulators [20]. This design can effectively land on irregular surfaces. After sensing the shape of the target surface through the sensor, the joints of each manipulator are set to fit the target surface. However, this design still has limitations on the landing angle, and it cannot land on an inclined plane above 40° including perpendicular surfaces. And in [15], Kamel *et al*. presented a mechanical design of UAV platform with a tiltable rotor. They demonstrated a transition from horizontal to upside flight and physical interaction with a wall. Their design is limited to land only on the planar surface. This way of design using the tiltable rotor technology might not be entirely feasible to land on irregular surfaces and the tiltable rotor also could experience a speed problem of slow rotor tilting. Also, maneuverability has become harder than conventional UAVs and it requires a higher battery power.

In [2], in order to make the UAV land on an inclined surface, Bass *et al*. proposed to use the reverse thrust of UAV to extend the landing slope, and it can nearly double the maximum inclination. Although the ability of the bidirectional rotor alone can make the UAV land on the inclined surface, for larger inclination angles and more complex real-world environments, it still needs to be completed with the lightweight robotic landing gear.

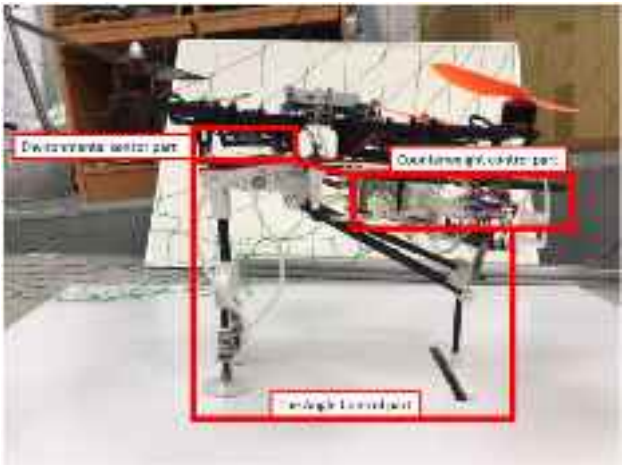

Fig. 1 Installation positions of angle control, counterweight, and sensor parts

3 Novel design for robotic landing gear

In this section, we provide details on the proposed robotic landing gear for off-the-shelf UAVs made up of 3 different parts: the angle control part (ACP), the counterweight control part (CCP), and the environmental sensor ppart (ESP). As a part of its modular design, the distance between the front leg and the rear leg can be adjusted according to users' needs and the size of the UAV. Specifically, responding to the mass distribution changes and the center of mass shifts, only the location of CCP needs to be adjusted backwards and forwards with respect to the servo motor position of the front leg prior to takeoff. This will allow the proposed landing gear to accommodate different-sized UAVs without any adverse impact on its landing capability. The type of UAV used is based on the DJI F450 frame with a brushless motor of 14.8V/9.5A-920 rpm/V. It has a very limited payload of 1 kg. The motivation behind using the UAV with such a low payload is to enforce our design as minimum as possible so that it can be used by any type of UAV with a payload capacity of more than 1 kg. The proposed robotic landing gear weighs only 900 g. The installation of these parts is shown in Fig. 1. The robotic legs are designed to be attached to the surface with a vacuum system. The CCP is composed of the rather heavy and essential parts: a vacuum motor and a battery. Since the landing gear is mounted underneath the UAV, the weight reduction and the center of gravity change adjustment become particularly important. Depending on both payload and size of the UAV, the position of the CCP can be adjusted manually when the landing gear is being attached to the UAV in such a way that it keeps the center of gravity of the UAV with the landing gear as close as possible to the center of the original UAV. The ESP is the place to install various types of sensors for intended applications (e.g., RGB-D camera, Lidar, Heading, IMU, and related others) in order to sense

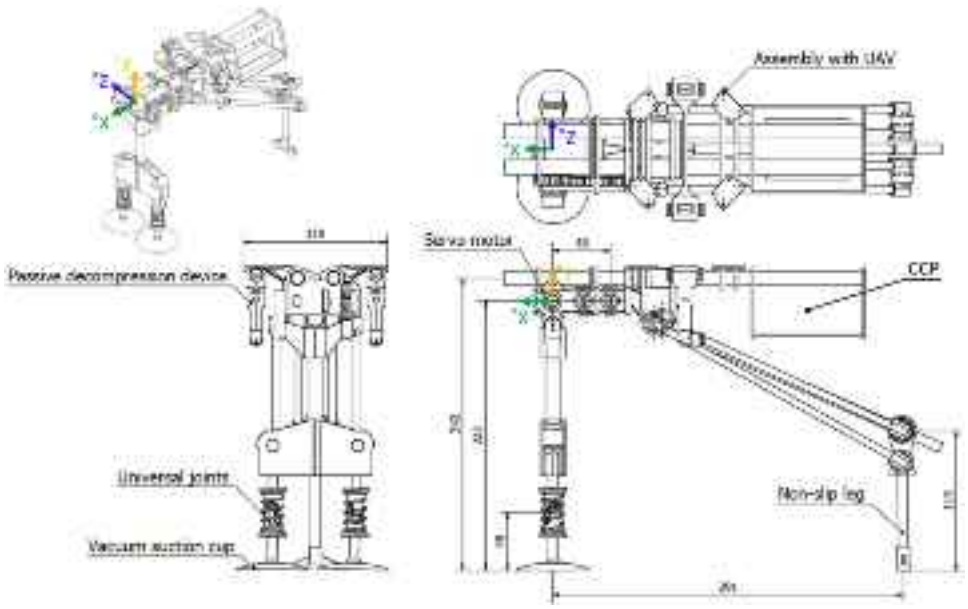

Fig. 2 The CAD drawing of the robotic landing gear. A servo motor controls the angle between the front leg and "X axis of the UAV

the target landing surface details, including the titling angle of the wall relative to the UAV approaching direction. In this paper, we focus on the ACP and mechanical structure design of the landing gear. The ACP consists of a servo motor with $25kgf \cdot pcm$ torque, two front robotic legs, and a non-slip leg. This design is inspired by the triangular landing gear designs used in commercial aircraft systems. Such triangular systems have been referred to as the most stable polygons. Two vacuum suction cups are mainly designed as a backup/emergency plan for any failure that might appear during landing and/or attaching to the surface. The CAD model of the prototype is shown in Fig. 2.

To better understand how the robotic landing gear can land on different shapes and inclinations of surfaces, we define the target surface in the world coordinate system (or the XYZ Cartesian axes) separately in the XY and XZ plane as illustrated in Fig. 3. While the robotic leg in the front accommodates the difference in surface shapes in the XZ plane, the front leg and the rear non-slip leg forms a closed-chain structure by attaching to the surface in the XY plane.

3.1 Design of the robotic legs

Each robotic leg has a vacuum suction cup with a 60 mm diameter, a set of universal joints, a compression spring, and a vacuum tube. Each suction cup can generate a suction force of 37.68 N collocation with a DC $12V$/0.4 A vacuum motor. The suction mechanism can withstand a maximum load of 10 kg under the 3D printing parameters (e.g., density, infill, the material used, and similar other parameters) we used. For different angles of inclination of landing surface, robotic legs work passively on adjusting the vacuum suction cup's angle when contacting the surface as shown in Fig. 4 automatically.

Since the robotic landing gear uses a vacuum system to keep the UAV attached to the surface, the vacuum suction cup must be perpendicular to the target surface to maximize the adhesive force. In order to adapt to the different shapes of the surface, this design allows the robotic leg to be kept perpendicular adaptively to the surface and attached to it. Moreover, it can also correct slight angle errors when landing. In terms of structural design, the universal joint can provide the vacuum suction cup with about 45° of steering in all directions. The steering degree of the universal joint is based on the shape of the target landing surface and the velocity of the UAV when approaching the target surface. The greater the velocity, the greater the rotation angle of the universal joint due to the compression spring used. The analysis of usable steering angle of the actual universal joint will be presented in the Experimental Results section. When the UAV needs to leave the target surface, the compression spring will return the vacuum suction cup to the original position for the next landing.

The two robotic legs in the front are separated into two sides using a torsion spring to keep them parallel. In this way, we can enable the robotic landing gear to land on different shapes of surface and achieve the cushioning effect by absorbing the shock during UAV landing. Even though the surface is not purely planar in the XZ plane, the torsion spring and the universal joint are flexible enough to accommodate different shapes of the surface. Some examples are shown in Fig. 5.

3.2 Structure of the front and rear legs part

The mechanical structure of the front leg and the rear leg adapts to the surface in the XY plane. Since a single motor

Fig. 3 The projection of a 3D surface onto the *XZ* and *XY* planes. The varying surface curvature appears as a curved line, such as the red line in the figure, from which the shape of surface can be coarsely defined. Using this line, the landing gear is set up to its landing configuration

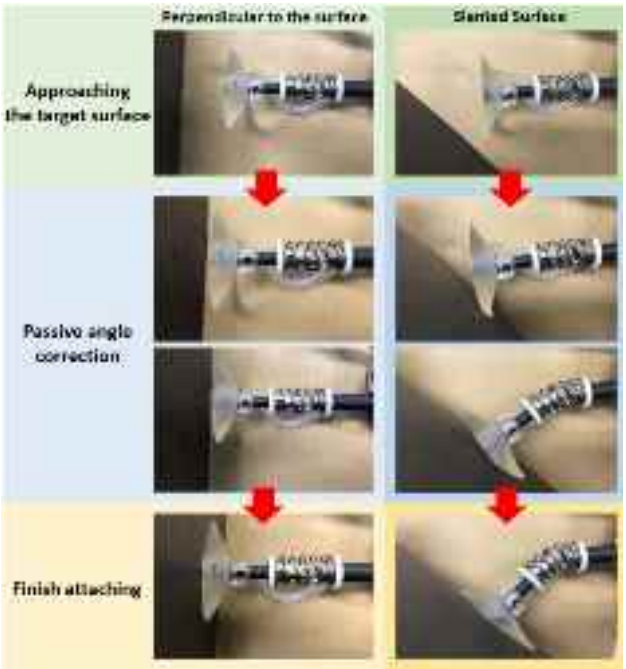

Fig. 4 Attaching to the target surface: When the soft rubber part of the vacuum suction cup touches the landing surface, the friction between the rubber and the surface will steer the universal joint, keeping the vacuum suction cup perpendicular to the surface

controls the angles of the front and rear leg configurations in ACP, in order to keep both legs parallel to the landing surface, we need to determine a gear ratio to make the non-slip rear leg rotate more than the front leg. Using the linkage method of multiple rods, the non-slip leg can change the angle and length with only a single motor input simultaneously. This design can make the front and rear legs have different angle changes, enabling them to adapt to the surface of different curvatures. Since the robotic landing gear uses a vacuum system to keep the UAV attached to the surface, it is important to ensure that the legs of the landing gear are perpendicular to the target surface. We define the ground plane as an angle of 0° surface and a vertical plane perpendicular to the ground as an angle of 90° surface. Our novel design structure can make the landing gear land between 0° and 100°. Regardless of any angle of inclination of the target surface, it can keep the 3 legs perpendicular to the target surface.

We assume that the angle of inclination of the target surface is α, Θ_1 is the angle controlled by the servo motor, Θ_2 is the angular position of the rear leg, and Θ_3 is the rotation angle of the rear leg to the surface. For the cases where $\Theta_1 \in (0, \pi/2]$, we can make use of triangular representations as shown in Fig. 6. Then the angular relationship between the target surface and the servo motor (front leg) is given by

$$\alpha + \Theta_1 = \frac{\pi}{2}. \tag{1}$$

The front leg and the rear leg are driven by a gear with a ratio of 1 : 1.28. This ratio is derived from the data obtained from simulations in the AutoDesk Inventor environment by modeling a linear relationship between Θ_2 and Θ_1. Therefore, the angle relationship between the front and the back leg is described by

$$\dot{\Theta}_2 = 1.28 \times \dot{\Theta}_1. \tag{2}$$

From the entire structure of the polygon with $n = 5$ sides, by using the formula for the sum of the interior angles $(n - 2) \times \pi$, the relationship between the Θ_3 and other angles can

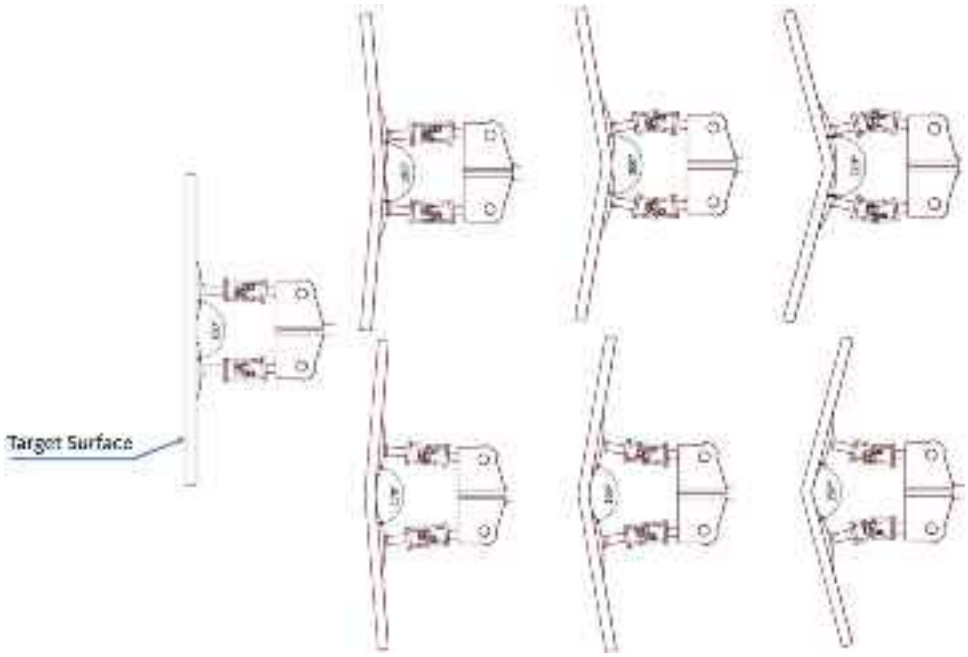

Fig. 5 The two front robotic legs are flexible enough to accommodate any shape in the *XZ* plane. The back leg is only to support the entire landing gear, therefore it will not affect the difference in the *XZ* plane

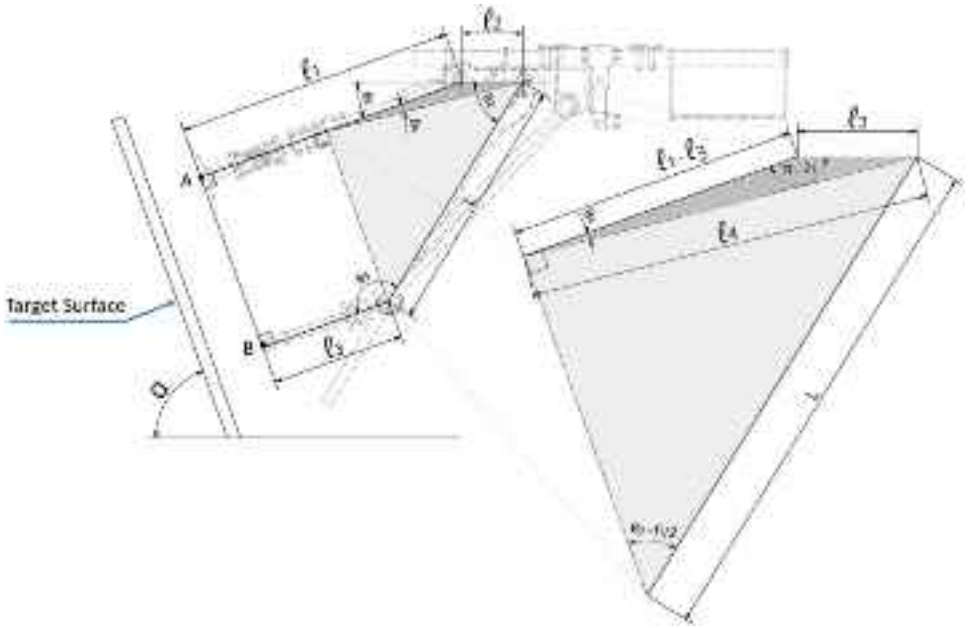

Fig. 6 This figure is the setup of landing gear for an example of the $\alpha = 70$ degree target plane. It shows the definition and position of each angle within the main structure

be written as follows:

$$\begin{aligned} \frac{\pi}{2} + \frac{\pi}{2} + \Theta_3 + \Theta_2 + \pi - \Theta_1 &= (5-2) \times \pi \\ \Theta_3 + \Theta_2 - \Theta_1 &= \pi \end{aligned} \tag{3}$$

With different surface inclination angles, the angle Θ_1 (thus, Θ_2 and Θ_3) and length L will change at the same time accordingly. To calculate the length L, we can first calculate ℓ_4 using the law of cosines in the dark gray triangle in Fig. 6.

$$\begin{aligned} \ell_4^2 &= (\ell_1 - \ell_3)^2 + \ell_2^2 - 2\ell_2(\ell_1 - \ell_3)\cos(\pi - \Theta_1) \\ &= (\ell_1 - \ell_3)^2 + \ell_2^2 + 2\ell_2(\ell_1 - \ell_3)\cos(\Theta_1) \end{aligned} \tag{4}$$

where ℓ_1, ℓ_2, and ℓ_3 are leg segment lengths. After computing ℓ_4, by using the law of sines, Θ_4 can be calculated as follows:

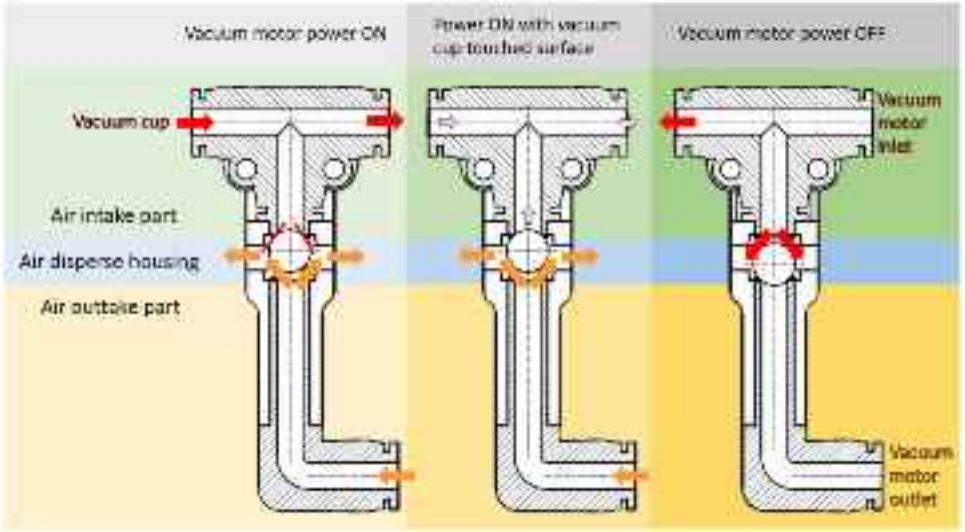

Fig. 7 When the vacuum motor is turned on, the small steel ball is blown upward by the air from the outtake part and blocks the intake part. Since this air intake part is connected in parallel with the vacuum suction cup, the small steel ball will not be fully blocking the air intake part until the vacuum suction cup is attached to the surface

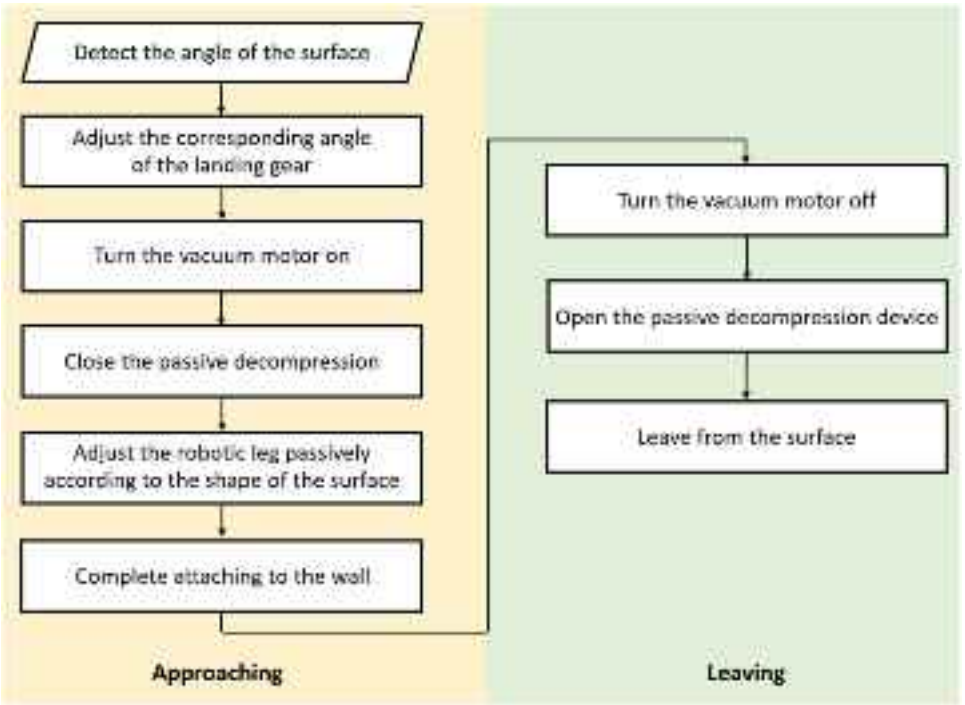

Fig. 8 A brief operation process of the landing gear divided into two parts: approaching and leaving. After leaving the current surface, return to the approaching part for next target surface landing

$$\frac{\ell_2}{\sin\Theta_4} = \frac{\ell_4}{\sin(\pi - \Theta_1)}$$
$$\Theta_4 = \sin^{-1}\left(\frac{\ell_2 \sin\Theta_1}{\ell_4}\right) \tag{5}$$

After calculating ℓ_4 and Θ_4, from the bigger triangle (colored light gray in Fig. 6), the length L can be calculated using the law of sines given by

$$\frac{L}{\sin(\frac{\pi}{2} - \Theta_4)} = \frac{\ell_4}{\sin(\Theta_3 - \frac{\pi}{2})},$$
$$L = \frac{\ell_4 \cos\Theta_4}{-\cos\Theta_3}. \tag{6}$$

With this design, for the surface in the XY plane to which the front and rear leg are positioned, any shape of the surface can be regarded as a plane with a different angle of inclination. The angle α with the ground plane can be calculated via a line segment connecting the landing points. Then Θ_1 can be

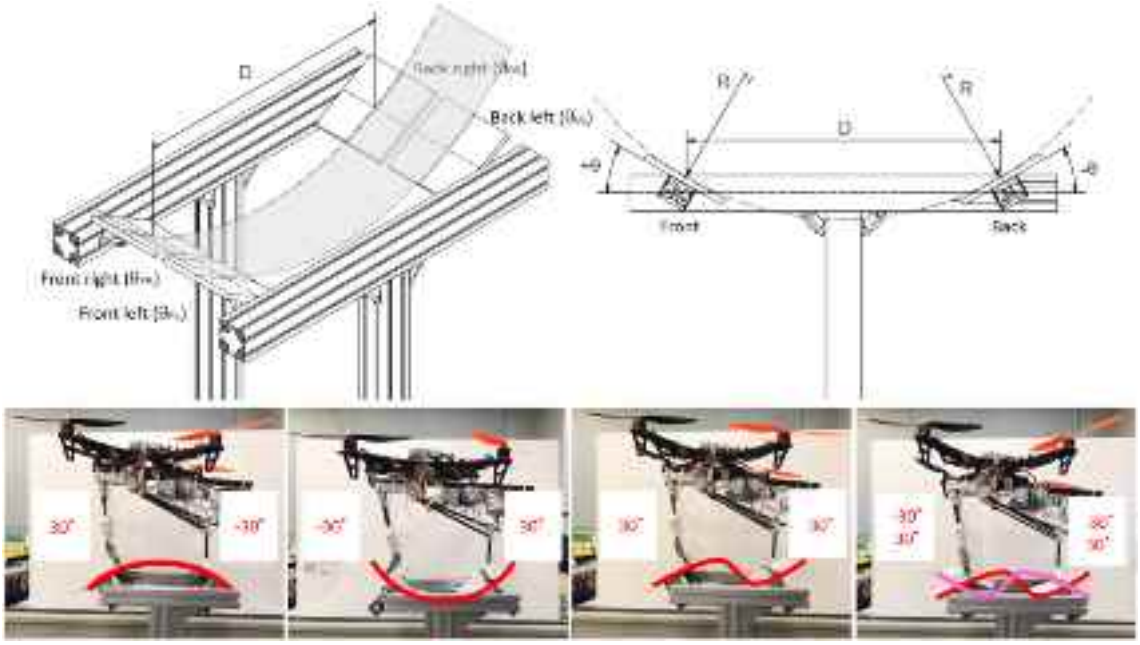

Fig. 9 The uneven landing terrain testbed to simulate different types of surfaces by changing the surface undulation angle. We define the angle change in clockwise direction as positive and counterclockwise as negative

set in such a way to keep the front and rear leg parallel to the landing surface. The universal joint at the front end of the robotic leg can passively perform a slight angle correction, according to the actual shape of the surface at the landing point. However, instead of using a robotic leg with a vacuum suction cup, the rear leg is designed to be a non-slip leg. From our experiments, it was noticed that when all the legs in contact with the target surface are equipped with universal joints, the structural rigidity is seriously insufficient and it could cause the landing gear to fall off the target surface easily. It would also cause the UAV to be unable to land in a horizontal attitude after the power is turned off. Also, when leaving the target surface, it could lead to a control loss when the UAV propellers start to rotate again. It also limits the types of target surfaces. For discontinuous surfaces, the success rate of landing would decrease due to insufficient rigidity. The advantages of designing the rear leg with a non-slip foot are not only to solve the aforementioned issues, but also not to affect the adsorption force of the vacuum system on the target surface. It has also a better landing effect for discontinuous surfaces.

3.3 Design of the passive decompression device

When the UAV needs to leave the surface, the vacuum system needs to be decompressed to release the vacuum environment so that the UAV can take off smoothly. For this reason, we design a passive decompression device as shown in Fig. 7. Compared to the electronic decompression device, the passive decompression device is lighter and less power-demanding, while preserving the necessary functionality. This passive decompression device is composed of three parts: the air intake part, the outtake part, and air disperse housing. The air intake part is connected to the air disperse housing, the vacuum suction cup, and the air inlet part of the vacuum motor. The air outtake part is connected to the air disperse housing and the air outlet part of the vacuum motor. The air disperse housing connects the intake part and outtake part and has a small steel ball in the center.

The outtake part will blow the small steel ball upward when the vacuum motor is turned on. Since the vacuum suction cup has not been attached to the target surface, the intake part will not become in a negative pressure state. Therefore, the part sucking the small steel ball has almost no suction for the small steel ball. This is because the vacuum suction cup and the sucking part are connected in parallel within the intake part. Therefore, until the vacuum suction cup is attached to the target surface, it will increase the suction power of the part that sucks the small steel ball and blocks it. And the intake part will be in negative pressure state to complete the suction step. When the UAV needs to leave the surface, it is only necessary to stop the vacuum motor. The small steel ball will quickly leave the air intake part, opening (the previously closed) air intake part. By doing so, the vacuum suction cup can be removed from the surface smoothly and quickly. While a small vacuum solenoid valve weighs around 50 grams, this passive pressure reduction unit weighs

Table 2 Success rate experimental trials for different type of surface

$\Theta_{FL} = \Theta_{FR}$ in degrees	$\Theta_{BL} = \Theta_{BR}$ in degrees	Contact area of non-slip leg	Success rate
0	0	Full	100%
10	10	Full	100%
20	20	Full	100%
30	30	Full	100%
40	40	Full	70%
50	50	Full	50%
10	−10	Full	100%
20	−20	Full	100%
30	−30	Full	100%
40	−40	Full	80%
50	−50	Full	70%
−10	10	Full	100%
−20	20	Full	100%
−30	30	Full	100%
−40	40	Full	80%
−50	50	Full	80%
−10	−10	Full	100%
−20	−20	Full	100%
−30	−30	Full	100%
−40	−40	Full	60%
−50	−50	Full	50%

Θ_{FL}	Θ_{FR}	Θ_{BL}	Θ_{BR}	Contact area	
				of non-slip leg	Success rate
−10	10	−10	10	Full	100%
−20	20	−20	20	Full	100%
−30	30	−30	30	Full	100%
−40	40	−40	40	Full	60%
−50	50	−50	50	Full	70%
−10	10	−10	10	Half	100%
−20	20	−20	20	Half	100%
−30	30	−30	30	Half	100%
−40	40	−40	40	Half	60%
−50	50	−50	50	Half	60%

only 9 grams. Since every extra weight means more power consumption for the motor of UAVs, we opted to use a passive pressure-reducing device in order to keep the proposed robot landing gear as light as possible. The passive pressure-reducing device not only requires no additional control but also is lighter.

3.4 The operational principle of robotic landing gear

A brief operation process is given in Fig. 8. Right after take-off, the ACP rotates the robotic legs up and makes them face front (the direction of flight) and keeps them horizontal. When approaching the target surface, the 3D shape of the surface is detected using the data provided by the sensor part and set up the robotic legs adjustments accordingly to start the vacuum system and be ready to approach the target surface. The decision of whether the robotic legs are fully attached to the surface or not is determined via the vacuum value. When taking off the surface again, the vacuum system is turned off and the power of the UAV is throttled to leave the surface.

Fig. 10 Some examples of landing on arbitrarily shaped surfaces. The landing gear can easily connect to a variety of surfaces with different curvatures through passive universal joints

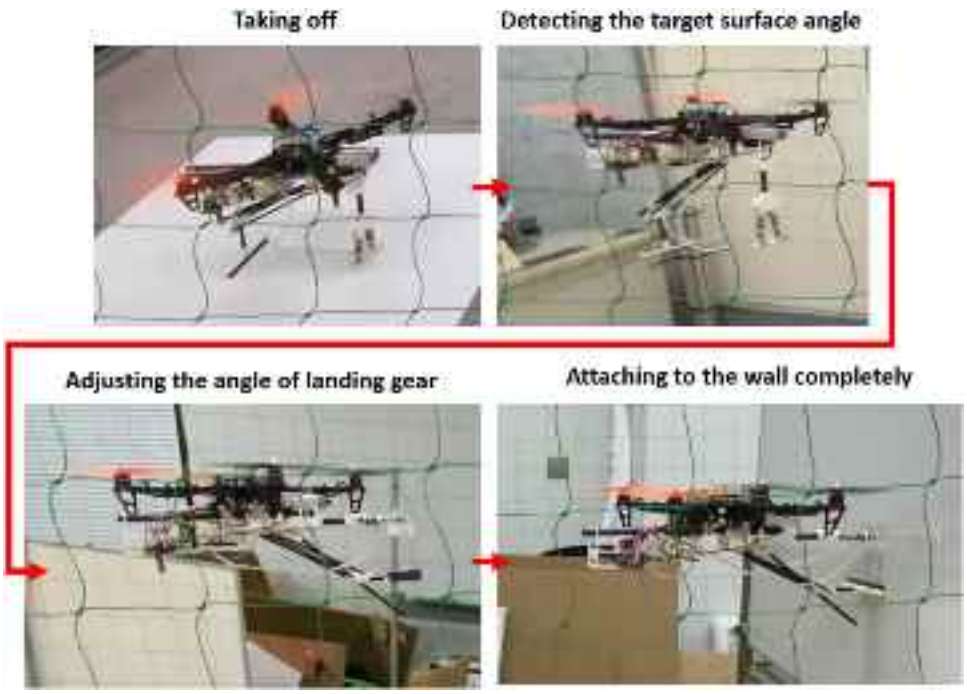

Fig. 11 The figure shows the operational principle of robotic landing gear. According to the calculation of the center of gravity of the entire UAV system, given the counterweight position pre-adjusted while the robotic landing gear was being attached to the UAV, the angle of the robotic legs changes during the flight without affecting the flight stability and balance control. A sample flight scenario can be seen at https://youtu.be/fbsFBl-dzFs

4 Experimental results

We carried out a preliminary landing experiment with an in-house built terrain generation system as shown in Fig. 9. This testbed allows creating different undulating surfaces by adjusting the angle of the landing plane. We also adjust test surfaces by calculating the distance between the front and rear legs. The limit curvature radius (R) of the surface can be calculated by using the angles (Θ_{FR}, Θ_{FL}, Θ_{Back}) and the distance (D).

During the experiments, we attached the robotic landing gear to a custom-built quadcopter based on commercially available DJI F450. After experimenting with various landing trials (10 for each angle combination), the success rate of the robotic landing gear for different types of surfaces is presented in Table 2. The first two columns denote the angle configurations used in the landing terrain testbed, referring to Fig. 9, while the third column represents the contact area between the non-slip leg and the surface being tested. As a result of experimental tests, the landing limits for the robot were within 50° of the tangent point of the irregular surface and $R \geq 200$ mm obtained by the geometrical relation $D = 2 \times R \times sin(\Theta)$. D changes depending on the UAV size and also the small variation caused by passive joints (see Figs. 4 and 12). In our case, D was approximately 300 mm. During the experiments, failed landing attempts have been observed

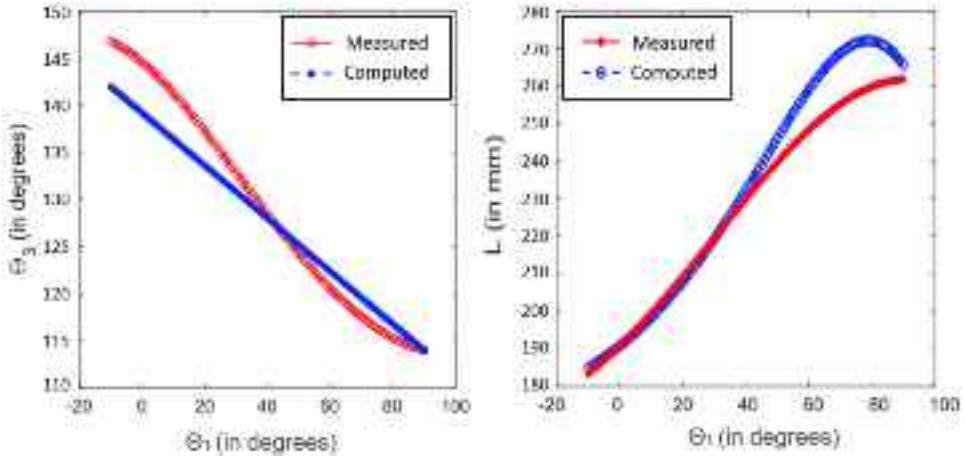

Fig. 12 These graphs denote computed values using Eqs. (1)–(6) and measured values during experiments for Θ_3 and L over Θ_1. Small discrepancy between values are mainly the right angle assumption between legs and the surface (points A and B in Fig. 6) since this assumption does not hold always due to the universal joint

when the tilt angles of both the front and back planes are very large and in the same direction. The reason is the lack of enough friction force generated by the vacuum cup material. That leads to making it difficult to guide the universal joint when it touches the landing surface. It was observed from the experiments that the rear non-slip leg design was able to land successfully regardless of the landing surface angle variations and unevenness of the landing surface.

We then proceed to the main experiments covering the entire flight and landing process. In our experiments, we use 6 different types of surfaces with smooth material (*e.g.*, plastics and metals) as shown in Fig. 10, including a vertical surface, a 45-degree slope surface, a discontinuous surface with elevation differences, and 3 types of curved surfaces with various radii of curvature, to test whether the robotic landing gear can successfully land on uneven surfaces. The whole operation process is divided into several steps: taking off, setting robotic legs to the initial position (defined by $\Theta_1 = 0$), approaching target surface, contacting target surface, and decreasing power. The overall pipeline of the experiment is given in Fig. 11.

We measured the Θ_3 and L distance during the landing experiments on different angled surfaces. We also computed the same values using Eqs. (1)–(6) and obtained values are given in Fig. 12. Some small error can be seen between values and this is mainly the right angle assumption between legs and the surface contact points. These errors are mostly compensated by the universal joints of front legs, demonstrating their importance in the proposed design. Since universal joints can compensate for some deviations from the right angle, the legs are not necessarily perpendicular to the surface all the time.

In order to make the universal joint automatically return to its original position, we use springs to perform the task of passive return. Among the ones we tested, we found that Ø1.4×19×55 and Ø1.2×20×40 were too soft, while Ø1.6×22×45 was too stiff to serve the intended purpose.

Table 3 Pressure relief time with and without passive decompression device

$\Theta_1 = \Theta_{FL} = \Theta_{FR}$ in degrees	Without device in seconds	With device in seconds
0	525	1.56
10	520	1.55
20	500	1.45
30	467	1.41
40	450	1.31
50	392	1.30
60	381	1.25
70	380	1.25
80	344	1.21
90	327	1.20
100	315	1.10

We also tested torsion springs that did not provide a successful outcome in all angles and a set of 3 tension springs that were also failed. We use Ø1.4×19×43 that were empirically found to be the best for our purpose and design.

We compared the decompression speed with and without the proposed passive decompression device. Table 3 shows the measured time for tested landing surfaces with different angles. For each surface angle, we measured 3 times and mean times are reported in the table. After turning off the power of the vacuum motor, without breaking the vacuum environment, the negative pressure in the vacuum suction cup continues for a very long time, making it difficult for the UAV to leave the surface. However, when the passive decompression device is installed, as soon as the vacuum motor is turned off, the negative pressure in the suction cup is released immediately, making the UAV leave the surface quickly.

When robotic legs are facing front while flying, the rotation speed of the landing gear is likely to affect the stability of the UAV. We did different experiments with rotating speed of the servo motor. In the first experiment, when the servo motor was set to rotate 95° in 3 seconds, the UAV has lost its balance and fell down. When the selected rotation time is about 5 seconds, the balance was still adversely affected, and the UAV suffered a short-term control failure. However, it did not fall down. When the selected rotation time is 10 seconds, the balance was affected slightly, but it did not affect the flight.

In order to test the landing ability on arbitrary surfaces, we set landing surface angle in view of *XZ* plane between [150°, 210°] with 5-degree intervals in the *XZ* plane simulating the cases depicted in Fig. 5. We performed 10 landing trials for each angle. We observed that the larger the angle, the more accurate speed and angle of the UAV control are required. The UAV control became very difficult when the angle is within the intervals [150°, 160°] and [195°, 210°]. For the rest of angles tested, the UAV has attached to the target surface easily. According to experiments, the front leg is designed for different angles and has an adaptive correction capability of about $\pm 20°$ of the target surface. The angle change greater than $\pm 20°$ from 180° will increase the difficulty of UAV control, and therefore such condition is normally not suitable for the proposed landing gear design.

5 Conclusions and future work

Over the last decade, an increasing number of studies have attempted to design various types of UAVs flying autonomously outfitted with different sensors and enable them to maintain stable contact with the environment for remote inspection and monitoring. Along the lines, this paper presented a novel robotic landing gear with 3 angle-adjustable robotic legs helping UAVs stick to the structure surface by a vacuum system. In the proposed design, the robotic landing gear allows the UAV to land on irregular surfaces. A passive angle adjustment method was adopted based on the mechanical structure to effectively reduce weight and power consumption. It was demonstrated through our laboratory experiments that this design can be easily connected to irregular surfaces such as uneven and curved surfaces.

For future work, we will aim at developing a cooperative flight control system with the robotic landing gear, allowing the robotic landing gear and surface contact interaction to transition in a more stable and safer way before and after connecting to the terrain.

Acknowledgements This material is based upon work supported by the U.S. Air Force Office of Scientific Research under AFOSR/AOARD FA2386-20-1-4019 Grant.

References

1. Albers A, Trautmann S, Howard T, Nguyen TA, Frietsch M, Sauter C (2010) Semi-autonomous flying robot for physical interaction with environment. In: 2010 IEEE conference on robotics, automation and mechatronics, pp 441–446. IEEE
2. Bass J, Desbiens AL (2020) Improving multirotor landing performance on inclined surfaces using reverse thrust. IEEE Robot Autom Lett 5(4):5850–5857. https://doi.org/10.1109/LRA.2020.3010208
3. Bisht R.S, Alexander S.J (2013) Mobile robots for periodic maintenance and inspection of civil infrastructure: a review. In: International conference on machines and mechanisms, pp 1050–1057
4. Dethe RD, Jaju S (2014) Developments in wall climbing robots: a review. Int J Eng Res Gen Sci 2(3):p33-42
5. Gago J, Douthe C, Coopman R, Gallego P, Ribas-Carbo M, Flexas J, Escalona J, Medrano H (2015) Uavs challenge to assess water stress for sustainable agriculture. Agricult Water Manag 153:9–19
6. Gómez-Candón D, De Castro A, López-Granados F (2014) Assessing the accuracy of mosaics from unmanned aerial vehicle (uav) imagery for precision agriculture purposes in wheat. Precis Agricult 15(1):44–56
7. González-deSantos LM, Martínez-Sánchez J, González-Jorge H, Arias P (2020) Active uav payload based on horizontal propellers for contact inspections tasks. Measurement 165:108106
8. Hallermann N, Morgenthal G (2014) Visual inspection strategies for large bridges using unmanned aerial vehicles (uav). In: Proceedings of 7th IABMAS, international conference on bridge maintenance, safety and management, pp 661–667
9. Ichikawa A, Abe Y, Ikeda T, Ohara K, Kishikawa J, Ashizawa S, Oomichi T, Okino A, Fukuda T (2017) Uav with manipulator for bridge inspection-hammering system for mounting to uav. In: 2017 IEEE/SICE international symposium on system integration (SII), pp 775–780. IEEE
10. Ikeda T, Yasui S, Fujihara M, Ohara K, Ashizawa S, Ichikawa A, Okino A, Oomichi T, Fukuda T (2017) Wall contact by octo-rotor uav with one dof manipulator for bridge inspection. In: 2017 IEEE/RSJ international conference on intelligent robots and systems (IROS), pp 5122–5127. IEEE
11. Iwamoto T, Enaka T, Tada K (2017) Development of testing machine for tunnel inspection using multi-rotor uav. J Phys Conf Ser 842:012068
12. Jarman M, Vesey J, Febvre P (2016) Unmanned aerial vehicles (uavs) for uk agriculture: creating an invisible precision farming technology. White Paper, July
13. Jimenez-Cano A, Heredia G, Ollero A (2017) Aerial manipulator with a compliant arm for bridge inspection. In: 2017 international conference on unmanned aircraft systems (ICUAS), pp 1217–1222. IEEE
14. Jung S, Shin J.U, Myeong W, Myung H (2015) Mechanism and system design of mav (micro aerial vehicle)-type wall-climbing robot for inspection of wind blades and non-flat surfaces. In: 2015 15th international conference on control, automation and systems (ICCAS), pp 1757–1761. IEEE
15. Kamel M, Verling S, Elkhatib O, Sprecher C, Wulkop P, Taylor Z, Siegwart R, Gilitschenski I (2018) Voliro: an omnidirectional hexacopter with tiltable rotors. arXiv:1801.04581
16. Mahmood S, Bakhy S, Tawfik M (2021) Propeller-type wall-climbing robots: a review. IOP Conf Ser Mater Sci Eng 1094:012106
17. Myeong W, Jung S, Yu B, Chris T, Song S, Myung H (2019) Development of wall-climbing unmanned aerial vehicle system for micro-inspection of bridges. In: 2019 international conference on robotics and automation (ICRA). IEEE

18. Myeong W, Myung H (2018) Development of a wall-climbing drone capable of vertical soft landing using a tilt-rotor mechanism. IEEE Access 7:4868–4879
19. Myeong WC, Jung KY, Jung SW, Jung Y, Myung H (2015) Development of a drone-type wall-sticking and climbing robot. In: 2015 12th international conference on ubiquitous robots and ambient intelligence (URAI), pp 386–389. IEEE
20. Paul H, Miyazaki R, Ladig R, Shimonomura K (2019) Landing of a multirotor aerial vehicle on an uneven surface using multiple onboard manipulators. In: 2019 IEEE/RSJ international conference on intelligent robots and systems (IROS), pp 1926–1933. IEEE
21. Pope MT, Kimes CW, Jiang H, Hawkes EW, Estrada MA, Kerst CF, Roderick WR, Han AK, Christensen DL, Cutkosky MR (2016) A multimodal robot for perching and climbing on vertical outdoor surfaces. IEEE Trans Robot 33(1):38–48
22. Ratsamee P, Kriengkomol P, Arai T, Kamiyama K, Mae Y, Kiyokawa K, Mashita T, Uranishi Y, Takemura H (2016) A hybrid flying and walking robot for steel bridge inspection. In: 2016 IEEE international symposium on safety, security, and rescue robotics (SSRR), pp 62–67. IEEE
23. Ridao P, Carreras M, Ribas D, Garcia R (2010) Visual inspection of hydroelectric dams using an autonomous underwater vehicle. J Field Robot 27(6):759–778
24. Sanchez-Cuevas PJ, Ramon-Soria P, Arrue B, Ollero A, Heredia G (2019) Robotic system for inspection by contact of bridge beams using uavs. Sensors 19(2):305
25. Song YK, Lee CM, Koo IM, Tran DT, Moon H, Choi HR (2008) Development of wall climbing robotic system for inspection purpose. In: 2008 IEEE/RSJ international conference on intelligent robots and systems, pp 1990–1995. IEEE
26. Tsukagoshi H, Watanabe M, Hamada T, Ashlih D, Iizuka R (2015) Aerial manipulator with perching and door-opening capability. In: 2015 IEEE international conference on robotics and automation (ICRA), pp 4663–4668. IEEE
27. Watanabe K, Nakatsuka T, Nagai I (2018) Production of a wall-climbing-type quadrotor and its experiment for verifying basic operations. In: 2018 IEEE international conference on mechatronics and automation (ICMA), pp 1850–1855. IEEE